Applied Surface Science 646 (2024) 158950

Contents lists available at ScienceDirect

Applied Surface Science

journal homepage: www.elsevier.com/locate/apsusc

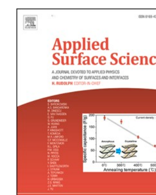

Full Length Article

High mobility and productivity of flexible In_2O_3 thin-film transistors on polyimide substrates via atmospheric pressure spatial atomic layer deposition

Kwang Su Yoo [a], Chi-Hoon Lee [a], Dong-Gyu Kim [a], Su-Hwan Choi [b], Won-Bum Lee [a], Chang-Kyun Park [c,*], Jin-Seong Park [a,*]

[a] Division of Materials Science and Engineering, Hanyang University, 222 Wangsimni-ro, Seongdong-gu, Seoul 04763, Republic of Korea
[b] Division of Nanoscale Semiconductor Engineering, Hanyang University, 222 Wangsimni-ro, Seongdong-gu, Seoul 04763, Republic of Korea
[c] Nano Convergence Leader Program for Materials, Parts, and Equipments, Hanyang University, 222 Wangsimni-ro, Seongdong-gu, Seoul 04763, Republic of Korea

ARTICLE INFO

Keywords:
Atmospheric spatial atomic layer deposition (AP S-ALD)
In_2O_3
Process parameters
oxide semiconductor thin film transistors (TFTs)

ABSTRACT

We fabricate In_2O_3 films using atmospheric pressure spatial atomic layer deposition (AP S-ALD) and investigate their properties at various temperatures (150 °C–225 °C). As the temperature increased, the growth per cycle (GPC) increases, with the GPC and refractive index reaching values of 1.33 and 2.02, respectively, at 225 °C. The In_2O_3 thin film indicates a reduction in carrier concentration from $1.53 \pm 1.37 \times 10^{21}$ to $3.09 \pm 0.53 \times 10^{20}$ cm^{-3} as the temperature increased, and a decrease in the resistance from $3.55 \pm 0.07 \times 10^{-3}$ to $3.70 \pm 0.01 \times 10^{-4}$ Ω•cm, which is attributed to a decrease in the impurity concentration (150 °C: 1.5 at.%; 175 °C: 1.0 at.%; 200 °C: N/A; 225 °C: N/A) and an increase in crystallinity. We use the In_2O_3 film as a channel layer in a top-gate bottom-contact thin-film transistor (TG-BC TFT). The device shows excellent performance characteristics, including a field-effect mobility of 69.8 cm^2/V·s, a threshold voltage of -0.06 ± 0.22 V, and a subthreshold swing of 0.16 ± 0.01 V/decade. We successfully fabricated high-mobility TFTs and demonstrated their reliability via bias and 50,000 bending tests. The high-performance channel layer of the TFTs fabricated using AP S-ALD are promising for flexible applications.

1. Introduction

Metal oxide semiconductors are attracting attention as an application field for active layers of thin film transistors (TFTs) and gas sensors and have excellent n-type characteristics. In addition, a lot of high-performance p-type field-effect transistors (FETs) research using metal chalcogenide has recently been conducted, and it is attracting much attention in high-performance electronics/optical electronics and emerging applications [1–3]. Indium oxide (In_2O_3) has received significant attention as a highly promising material for transparent conductive oxide (TCO) applications in next-generation electronic devices because of its superior electrical and optical properties, such as high electron mobility, high carrier concentration, and wide bandgap [4–7]. Various fabrication methods for In_2O_3 have been investigated extensively, including evaporation [8,9], sol–gel [9,10], spray pyrolysis [11–13], sputtering [13–15], chemical vapor deposition (CVD) [16–19], and atomic layer deposition (ALD) [20–23]. Currently, physical vapor deposition (PVD) techniques such as evaporation and sputtering are widely employed in commercial applications for the deposition of In_2O_3 and ITO thin films. However, they may not be suitable for coating complex three-dimensional (3D) substrates with high aspect ratios. ALD is a highly promising technique for depositing conformal thin films. During ALD, gaseous precursors are selectively adsorbed onto reactive sites via physical and/or chemical interactions, whereas unreacted precursors are purged. Subsequently, reactants are introduced to react with the adsorbed precursors, thus resulting in the growth of one atomic layer at a time. The self-limiting and atomic-level nature of the chemical reactions in ALD ensures superior film conformality across large areas and a precise control of the film thickness.

Despite the superior properties of In_2O_3 films deposited using ALD,

* Corresponding authors at: Nano Convergence Leader Program for Materials, Parts, and Equipments, Hanyang University, 222 Wangsimni-ro, Seongdong-gu, Seoul, Republic of Korea. (Chang-Kyun Park); Division of Materials Science and Engineering, Hanyang University, 222 Wangsimni-ro, Seongdong-gu, Seoul, Republic of Korea (Jin-Seong Park).

E-mail addresses: ckpark@hanyang.ac.kr (C.-K. Park), jsparklime@hanyang.ac.kr (J.-S. Park).

https://doi.org/10.1016/j.apsusc.2023.158950
Received 3 October 2023; Received in revised form 15 November 2023; Accepted 17 November 2023
Available online 19 November 2023
0169-4332/© 2023 Elsevier B.V. All rights reserved.

such as high uniformity and excellent conformality, the low growth rate of ALD, which is approximately 0.1 nm/s, may not satisfy certain industrial requirements. The limitations of ALD have been effectively addressed by the development of spatially separated ALD, which is also known as spatial ALD (S-ALD). S-ALD involves four distinct zones separated by an inert gas: precursor dosing, precursor purging, reactant dosing, and reactant purging. Both the precursor and reactant are continuously introduced and purged from separate zones, while a moving substrate is passed through each zone to facilitate rapid chemical reactions between the adsorbed precursor and reactant without requiring time-consuming purging steps. This allows the purge times to be reduced significantly. Meanwhile, advanced deposition methods must be devised to satisfy the increasing demand for flexible displays. Therefore, researchers have developed S-ALD [24,25], which involves roll-to-roll/sheet-to-sheet processes and high-throughput processes with low investment costs. Meanwhile, studies regarding the deposition of In_2O_3 via atmospheric pressure spatial atomic layer deposition (AP S-ALD) are insufficient.

Problems regarding the reproducibility of vapor control and the transfer of conventional solid indium precursors have emerged. In recent years, the development of new and improved liquid indium precursors for use in oxide–semiconductor applications has been actively investigated. Indium precursors reported in the literature include ethylcyclopentadienyl indium (In-EtCp) [26], acac = acetylacetonate, pentane-2,4-dione ($In(acac)_3$) [21], diethyl [1,1,1-trimethyl-N-(trimethylsilyl)silanaminato]-indium (INCA) [27–29], and, [3-(dimethylamino-kN)propyl-kC]dimethyl-indium (DADI) [30,31]. These precursors generally exhibit low growth per cycle, indicating low reactivity. If the reactivity is low, then impurities may be detected in the thin film and the crystalline phase may be degraded, thereby degrading the electrical properties. Continuous flow is realizable in AP S-ALD using a highly reactive liquid precursor. High-performance In_2O_3 thin-film transistors (TFTs), which are used in high-end display products, require high levels of mechanical stability, flexibility, and electrical conductivity for commercialization. Therefore, the electrical and mechanical stabilities of the In_2O_3 TFTs were evaluated to determine their feasibility for practical applications. Finally, for applications in the display industry, a study was conducted to investigate the component layers (buffer layer, active layer, and gate insulator) of the backplane using a highly productive AP S-ALD method.

In this study, we systematically investigate the effect of deposition temperature on the growth per cycle, impurities, and structural, electrical, and morphological properties of In_2O_3 thin films deposited via AP S-ALD using a novel liquid TMI(Trimethylindium) precursor. We use various analytical techniques, including Hall measurements, X-ray photoelectron spectroscopy (XPS), X-ray reflectometry (XRR), atomic force microscopy (AFM), X-ray diffraction (XRD), and wide-angle X-ray scattering (WAXS), to investigate the properties of the In_2O_3 thin films. Additionally, we evaluate the electrical and mechanical stabilities of the In_2O_3 thin films by applying TFTs and performing bending tests. The results obtained in this study can facilitate the optimization of the deposition conditions for AP S-ALD and improve the performance of In_2O_3-based electronic devices fabricated via the method, including flexible and wearable electronic devices, transparent electrodes, and optoelectronic devices.

2. Material and methods

2.1. *In_2O_3 deposition via AP S-ALD*

As shown in Fig. 1(a), We performed AP S-ALD using an equipment capable of processing 6-inch wafers (Nexusbe Co., Ltd.) [32]. Trimethylindium (TMI) (Solution TMI 40 °C, supplied from Lake Materials Co., Ltd.) and O_3 were used as the indium precursor and reactant,

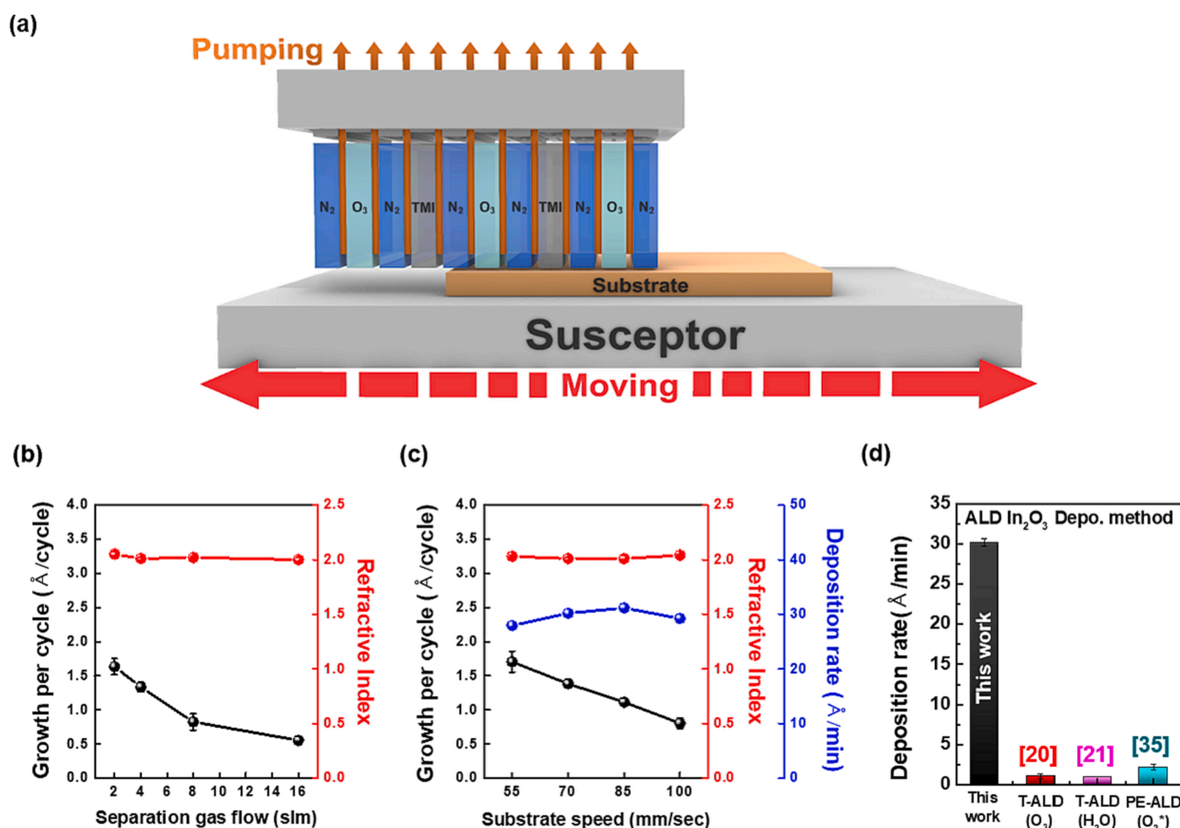

Fig. 1. GPC and RI of as-deposited In_2O_3 films based on (a) AP S-ALD equipment schematic (b) separation gas flow and (c) substrate speed. (d) Deposition rate of In_2O_3 film using AP S-ALD (In_2O_3 films using O_3, H_2O, and O_2 plasma reactants in conventional ALD are included as reference).

respectively, with N_2 (99.999 %) used as the separation gas and carrier gas for the precursor. Owing to the nature of S-ALD, we prioritized certain process. First, we confirmed the flow rate of the separation gas (2–16 slm) and the substrate velocity (55–100 mm/s) to ensure that the precursor and reactant were not mixed. Subsequently, we investigated the dose saturation characteristics of TMI (60 %–100 %) and O_3 (10 %–100 %). Finally, we established a window for the ALD process to ensure reproducibility and temperature dependency (150 °C–225 °C).

2.2. Fabrication of TG-BC In_2O_3 TFT

We deposited a 50 nm buffer layer of Al_2O_3 on a polyimide (PI)-coated glass substrate via AP S-ALD at 250 °C. Source and drain electrodes were deposited onto the buffered substrate by RF sputtering a 100 nm ITO layer, and patterned using conventional photolithography and wet etching processes. We deposited a 10 nm In_2O_3 active layer at different process temperatures using AP S-ALD and patterned it using conventional photolithography and wet etching processes. The gate insulator was fabricated by depositing a 50 nm Al_2O_3 layer via AP S-ALD at 250 °C, followed by opening contact holes for the source and drain. Subsequently, we deposited a 100 nm ITO layer using RF sputtering and patterned it using a conventional photolithography process to define the gate electrode. To improve the contact between the active layer and source/drain, we baked the sample on a hot plate in air at 125 °C for 15 min. The device channel used in the measurement had a width of 40 µm and a length of 20 µm. The electrical properties of the TFT were measured in a dark atmospheric pressure environment using the TOP Engineering S3000 electrical parameter analyzer, and the transfer curve was obtained by sweeping the gate voltage from −10 to 10 V at drain voltages of 0.1 and 5.1 V.

2.3. Characterization of In_2O_3 films

The thickness and refractive index of In_2O_3 thin films deposited using AP S-ALD were determined through spectroscopic ellipsometry (SE; Elli-SE(UV)-FM8, Ellipso Technology). For assessing the electrical properties, including carrier density, Hall mobility, and resistivity, Hall measurements were conducted using the HMS-5500 instrument from Ecopia. Using X-ray photoelectron spectroscopy (XPS, K-alpha+, Thermo Scientific) using an Al Kα (1486.6 eV) source with a pass energy of 50 eV and a beam size of 400 um, the oxygen chemical bond state and atomic composition ratio of the In_2O_3 thin film are analyzed. X-ray diffraction (XRD) was performed using the 2-θ method at a glancing angle of 1° in ambient air. A monochromatic X-ray with a wavelength of 1.2398 Å (~10 keV) and a size of 100 µm was generated using a DCM (double crystal monochromator) with bent Si (1 1 1) crystals. Furthermore, grazing-incidence wide-angle X-ray scattering (GIWAX) was utilized to investigate the orientation and ordering of the In_2O_3 crystallites. The interplanar distance (d) of crystals was calculated using the scattering vector (q) with the equation $d = 2\pi/q$. Both XRD and GIWAXS measurements were performed at the 3D and 3C beamline of Pohang Light Source II (PLS-II) in Pohang, Republic of Korea. X-ray reflectometry (XRR) was conducted with a Cu-Kα (1.5405 Å) target using a SmartLab instrument from Rigaku. The XRR analysis angle ranged from 0 to 10° with a step size of 0.005°, and the scan speed angle was set at 0.5°/min. Atomic force microscopy (AFM) was employed for assessing surface roughness and morphology using the XE-100 from Park System Co. All substrates used in the analysis were thermally grown SiO2 substrates. Finally, using the bending evaluation equipment of the Yuasa System, the radius was 5 mm, and it was evaluated at a speed of 35 rpm.

3. Results and discussion

In S-ALD, creating a spatially separated environment for the precursor and reactant is crucial to minimize CVD-like reactions caused by gas mixing. As shown in Fig. 1(b), the growth per cycle (GPC) and refractive index (RI) were evaluated under N_2 separation gas flow. The process temperature was fixed at 225 °C, and the substrate moving speed was fixed at 70 mm/s. The thickness of the In_2O_3 films was 30 nm. Within the separation gas flow region, the RI remained relatively stable regardless of the type of separation gas used. However, as the separation gas flow rate increased, the GPC decreased. As the separation gas flow increased, the precursor dosing efficiency decreased, thus resulting in a decrease in the GPC [33]. At a separation gas flow rate of 2 slm, the GPC increased but the uniformity of the film deteriorated. This can be explained by the insufficient separation N_2 flow for mixing the precursor and reactant, which consequently resulted in a CVD-like reaction [33,34]. To evaluate the productivity of the AP S-ALD based on a flow rate of 4 slm, we measured the GPC, RI, and deposition rate in the substrate speed range of 55–100 mm/s, as shown in Fig. 1(c). The RI did not vary significantly with the substrate speed for each speed tested. At a substrate speed of 85 mm/s, the deposition rate was the highest; however, the GPC decreased as the substrate speed increased. As the substrate speed increased, the exposure times of the precursor and reactant decreased, thus resulting in a decrease in the GPC. At a substrate speed of 55 mm/s, the film uniformity deteriorated as the GPC increased. This appears to be caused by the precursor condensation effect as the exposure time of the precursor increases [35]. We conjectured that a suitable spatially separated environment can be created under a 4 slm separation gas flow, and that uniform thin films can be obtained with excellent yield at a substrate speed of 70 mm/s. As shown in Fig. 1(d), we compared the deposition rates at a separation gas flow of 4 slm and a substrate speed of 70 mm/s using various In_2O_3 ALD methods. This comparison confirms that the deposition rate of AP S-ALD is approximately 30 times faster than that of conventional ALD (H_2O, O_3, and O_2 plasma) [22,23,36,37].

To confirm the range of the self-limiting behavior of the precursor and reactant, we measured the GPC and RI under various TMI and O_3 partial pressures, as shown in Fig. 2(a) and (b). We set the separation gas flow to 4 slm, the substrate speed to 70 mm/s, and the process temperature to 225 °C. The total flow rates of TMI and O_3 supplied by the injector were constant at 100 sccm. We supplied N_2 as a dilution gas for TMI and O_3, and then varied the TMI partial pressure from 60 % to 100 % and the O_3 partial pressure from 10 % to 100 % by adjusting the bubbler N_2 flow rate and dilution N_2 flow rate. The TMI and O_3 saturated at partial pressures of 80 % and 40 %, respectively. Based on the saturation behavior at each partial pressure, the film thicknesses were measured after 100, 200, and 300 cycles, as shown in Fig. 2(c). Based on experimental data, we performed a linear curve fitting to calculate the GPC of the 1.46 Å/cycle. By maintaining an appropriate temperature for sufficient reaction between TMI and O_3 and creating an appropriate spatial separation environment to suppress CVD-like reactions, we obtained a linear curve corresponding to the ALD cycle. Fig. 2(d) shows the GPC and RI values from 150 °C to 225 °C. As the process temperature increased, the RI remained at approximately 2.0, whereas the GPC increased. The increase in GPC with temperature can be attributed to the enhanced reactivity with O_3. The reaction between TMI and O_3 at low temperatures did not completely remove the methyl ligands of TMI. The unremoved methyl ligands served as steric hindrances that interfered with the adsorption of other TMI precursors, which decelerated film growth and decreased the GPC. As the process temperature increased, the reactivity between TMI and O_3 increased; consequently, more methyl ligands of TMI were removed, thus resulting in a higher GPC [38]. Additionally, to preclude the effect of precursor decomposition on the increase in the GPC, we perform a decomposition test. The decomposition test was conducted by injecting only the TMI precursor without any co-reactants, and the results showed no film growth up to 250 °C. We observed ALD behaviors within a narrow range of temperature, which is consistent with the results of previous studies [29]. We further investigated the changes in the film properties as a function of temperature.

We confirmed the change in the GPC based on the process

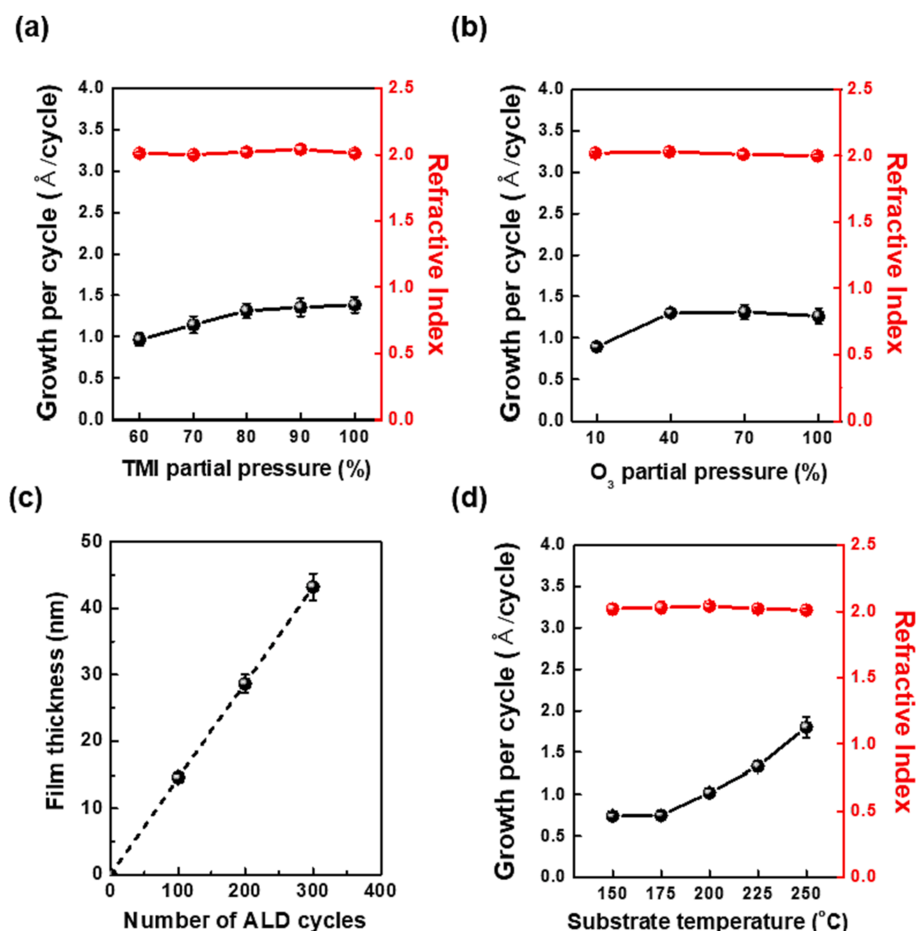

Fig. 2. Self-limiting behavior of (a) TMI partial pressure and (b) O_3 partial pressure (c) linear curve fit and (d) ALD window for varying substrate temperatures. AP S-ALD-fabricated In_2O_3 film has a narrow ALD window.

temperature, which resulted in variations in the electrical characteristics of the In_2O_3 films owing to discrepancies in the growth mechanism of the thin films. The carrier concentration, resistivity, and Hall mobility of the In_2O_3 films were determined via Hall measurements to evaluate their electrical properties with respect to the process temperature, as shown in Table 1. The thickness of In_2O_3 for Hall measurement was fixed at 10 nm. A relatively high carrier concentration was measured at 150 °C and 175 °C. The difference in reactivity depending on the process temperature can affect the chemical composition of the In_2O_3 films and thus the carrier concentration. Therefore, we expected C impurities to be present in the films because of their low reactivity with O_3. Several reports indicated that C impurities can serve as donors and increase the carrier concentration in films [39,40]. As the process temperature increased, the Hall mobility increased from 1.15 to 54.7 cm^2/Vs. The increase in the Hall mobility of In_2O_3 with the process temperature can be attributed to the effect of crystallinity. To further understand the properties of the In_2O_3 films, one must analyze their chemical composition and crystalline structure.

The chemical compositions of the as-deposited films were determined based on peak area analysis via XPS (see Table 2). The TMI precursor was composed of a metal cation and methyl ligands, including carbon and hydrogen. Therefore, at low processing temperatures, carbon-based impurities may exist within the film because of insufficient reactivity. Carbon was detected at 150 °C and 175 °C, whereas it was not detected at 200 °C and 225 °C, as shown in Fig. S1. Additionally, the O/In ratio approached the ideal stoichiometric ratio of ~1.5 after surface etching was performed. However, it is necessary to conclude the characteristics of the In_2O_3 thin film through additional analysis of chemical bonds according to deposition temperature, respectively.

As shown in Fig. 3(a), we conducted XPS O 1s peak measurements using XPS analysis to verify the oxygen bonding states of the In_2O_3 films at different process temperatures. The O 1s peak was deconvoluted into three subpeaks. (Fig. S2), where each subpeak represented O–In bonding, oxygen deficiency, and O–C and H bonding. The peaks were

Table 1
Electrical properties of In_2O_3 films based on process temperatures of 150 °C, 175 °C, 200 °C, and 225 °C. Carrier concentration, resistivity, and Hall mobility of the films were measured using Hall measurement.

Deposition Temperature (°C)	Carrier concentration ($N \times 10^{20}$ cm^{-3})	Resistivity ($\rho \times 10^{-4}$ Ω cm)	Mobility (cm^2/Vs)
150	15.3 ± 1.37	35.5 ± 0.07	1.15 ± 0.02
175	8.07 ± 1.27	2.05 ± 0.01	37.8 ± 0.08
200	3.45 ± 0.70	4.08 ± 0.02	44.4 ± 0.20
225	3.09 ± 0.53	3.70 ± 0.01	54.7 ± 0.20

Table 2
Atomic ratios of In, O, and C contents in the In_2O_3 films, which were fabricated at 150 °C, 175 °C, 200 °C, 225 °C. The O/In ratio was estimated in both cases, before and after ion beam surface etching.

DepositionTemperature (°C)	Atomic composition (%)			O/In ratio	
	Indium	Oxygen	Carbon	Before	After
150	40.0	58.5	1.5	1.9	1.5
175	40.6	58.4	1.0	1.7	1.4
200	40.7	59.3	N/A	1.7	1.4
225	40.9	59.1	N/A	1.7	1.4

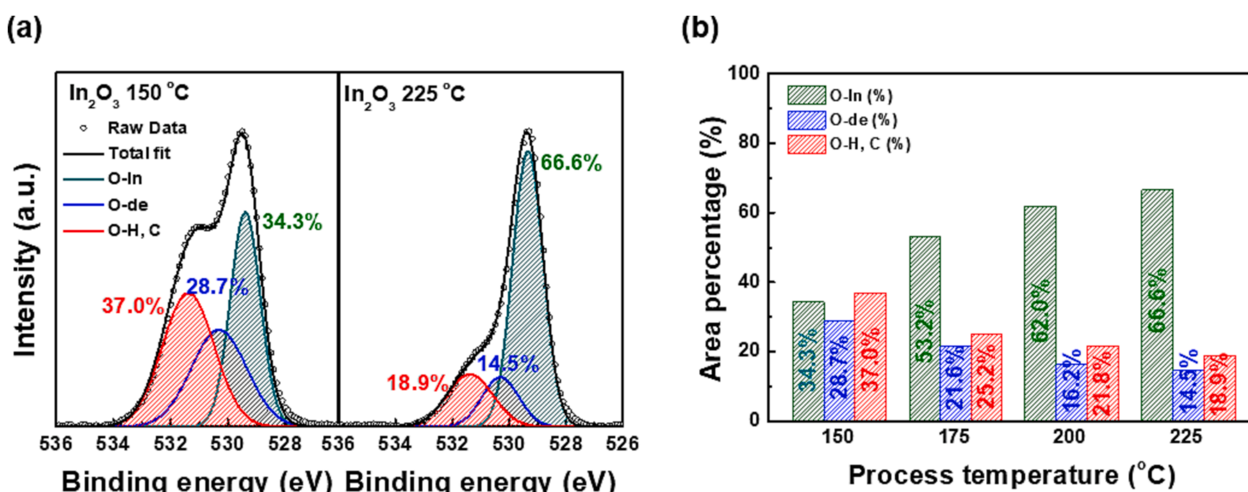

Fig. 3. XPS data for (a) O 1s of In_2O_3 films at 150 ℃ and 225 ℃ (c) Area fraction of oxygen-related bonds. Increase in carrier concentration with decreasing growth temperature is caused by residual C impurity.

positioned at 529.38 ± 0.03, 530.33 ± 0.01, and 531.39 ± 0.02 eV, respectively. Fig. 3(b) shows the area ratios of each subpeak in the temperature range of 150 °C–225 °C of In_2O_3. As the process temperature increased from 150 °C to 225 °C, the O–In ratio increased from 34.3 % to 66.6 %, the O–de ratio decreased from 28.7 % to 14.5 %, and the O–H, C ratio decreased from 37.0 % to 18.9 %. The trends in the changes of these subpeak area ratios may be correlated with the effect of the process temperature on the crystallinity of In_2O_3. As a result, O-In bonds increased at high temperatures, and oxygen defects and impurities decreased due to differences in activation energy depending on temperature. On the contrary, at low temperatures, the opposite trend was confirmed.

To explain the enhancement in the Hall mobility as the process temperature increased, we conducted crystallinity analysis on the In_2O_3 films. First, we analyzed the crystallinity of the as-deposited In_2O_3 films (see Fig. 4(a)). At 150 °C and 175 °C, smooth curves observed, thus indicating the amorphous nature of the films. By contrast, the phase of In_2O_3 films deposited at 200 °C and 225 °C indicated a bixbyite cubic structure (JCPDS card # 76-0152). Furthermore, we observed an increase in the (222)/(400) intensity ratio as the process temperature increased, as shown in the inset of Fig. 4(a). In fact, the (222)/(400) intensity ratio indicated the preferential growth of the (222) plane, which can be explained by the lower surface energy of the (111) plane compared with that of the (100) plane [41]. Therefore, at a high temperature of 225 °C, preferential growth occurred on the (222) plane because of the increased reactivity between the precursor and O_3. We conducted GIWAX analysis to investigate the correlation between the increase in the (222)/(400) intensity ratio and the crystallographic orientation, as shown in Fig. 4(b)–(e). At 150 °C and 175 °C, a faint ring pattern was observed, thus indicating the presence of nanocrystalline structures; hence, the film was almost amorphous, which is consistent with the GIXRD results. At 200 °C, the growth was randomly oriented, which formed a ring pattern on the (222) plane. At 225 °C, the (222) plane indicated preferential orientation, as compared with the case at 200 °C. The intensified growth and orientation of the In_2O_3 (222) plane with the increase in the process temperature improved the packing density of the film. This is because edge sharing was suppressed on the (400) plane in the cubic structure of In_2O_3, whereas corner sharing enhanced on the (222) plane. Improvement in the packing density through the preferential growth of the (222) plane can enhance the mobility of the film via the formation of longer conduction paths [42]. Furthermore, several studies have reported the preferential growth of the (222) plane in In_2O_3 at high temperatures [36,37].

As shown in Fig. 5(a), the XRR confirmed that the film density increased with the growth of the (222) plane, which intensified as the process temperature and packing density increased. As the process temperature increased from 150 °C to 225 °C, the film density increased from 6.56 to 7.09 g/cm^3. Moreover, the crystallization of the In_2O_3 film

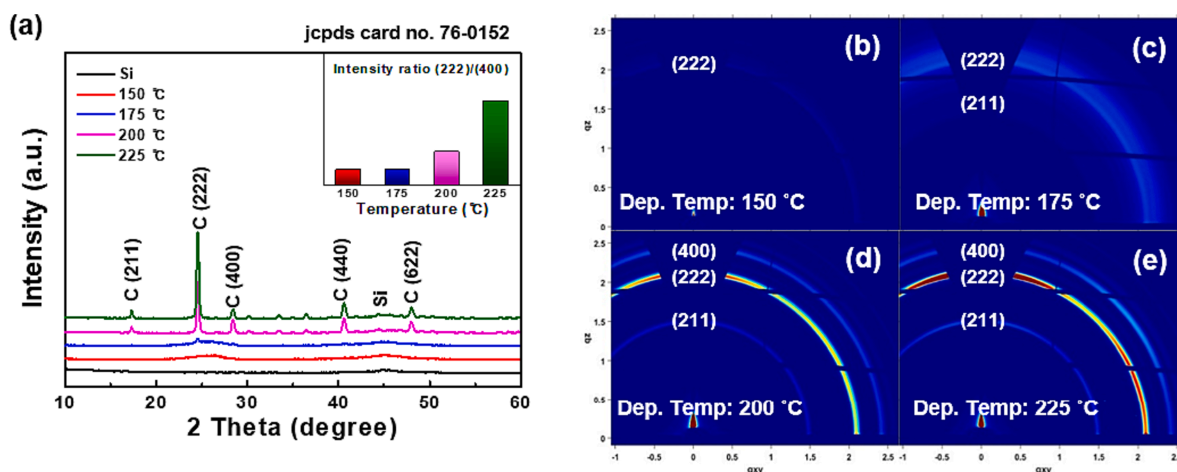

Fig. 4. (a) GIXRD patterns of In_2O_3 films deposited at different process temperatures. (b) GIWAX for deposition temperatures of (b) 150 °C, (c) 175 °C, (d) 200 °C, and (e) 225 °C. Bixbyite structure of In_2O_3 was clearly observed as temperature increased.

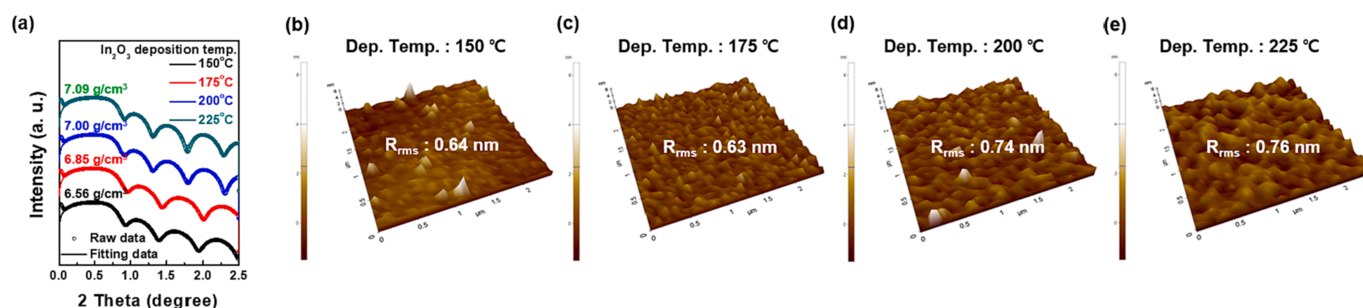

Fig. 5. (a) XRR analysis results for In_2O_3 film density and AFM 3D images of In_2O_3 films deposited at (b) 150 °C, (c) 175 °C, (d) 200 °C, and (e) 225 °C. The film density and surface roughness increase can be attributed to decreased impurity concentration and increased crystal orientation with increasing temperature.

can deteriorate the film surface roughness. The surface roughness of each In_2O_3 film was measured using AFM, as shown in Fig. 5(b)–(e). The film roughness values of the In_2O_3 films were 0.64, 0.63, 0.74, and 0.76 nm. The thickness of the In_2O_3 film used for the measurement was 30 nm and its roughness was ~2.3 %.

As shown in Fig. 6(a), we fabricated TFTs with a top-gate bottom-contact structure using In_2O_3 film as the active layer. In device fabrication, Al_2O_3 deposited via AP S-ALD is typically used as the buffer layer and gate insulator. We only conducted baking using a hot plate for 15 min in air to improve the contact between the source/drain and active layer. The transfer characteristics of the fabricated devices are presented in Fig. 6(b). The 150 °C In_2O_3 TFT did not exhibit switching characteristics as it transformed into a conducting TFT, as shown in Fig. S3. The In_2O_3 TFTs fabricated at 175 °C–225 °C exhibited stable switching characteristics. The electrical parameters of the devices are listed in Table S1. The In_2O_3 TFTs processed at 150 °C and 175 °C, which contained carbon-based impurities, showed conductance; as the carbon-based impurities decreased, switching characteristics were observed at

Fig. 6. (a) Schematic illustration of In_2O_3 TFT fabricated on PI substrate via AP S-ALD. (b) I_d–V_g characteristics of the In_2O_3 TFTs. (c) ΔV_{TH} as a function of Positive Bias Stress (PBS) time of the TFTs. TFTs based on the AP S-ALD-fabricated In_2O_3 films exhibited non-stable V_{TH} shifts due to grain boundaries formed by polycrystalline structures.

175 °C. At process temperatures of 200 °C and 225 °C, stable switching characteristics were observed near $V_{TH} = 0$. As the process temperature increased from 175 °C to 225 °C, the μ_{FE} increased. The trends of V_{TH} and μ_{FE} were consistent with the results of carrier concentration and Hall mobility obtained from the Hall measurements. Additionally, normal output characteristics were identified in Fig. S4. We evaluated the instability behavior of the In_2O_3 TFTs under a gate electric field of 1 MV/cm for 3600 s, as shown in Fig. 6(c). As the process temperature increased from 175 °C to 200 °C, ΔV_{TH} increased, which can be attributed to the grain boundary effect. At 200 °C, the formation of the In_2O_3 polycrystalline phase can degrade the reliability as electrons can be trapped at the grain boundaries. The deterioration of device performance owing to the grain boundary effect has been reported in previous studies [43,44]. As the process temperature increased up to 225 °C, the O–de ratio decreased. Therefore, because of the reduction in V_O, which serves as a charge trap, ΔV_{TH} can be improved [45,46].

To assess the stable electrical characteristics for flexible applications, we conducted bending tests on the In_2O_3 TFT at a temperature of 225 °C. The PI substrate used in the tests was delaminated from the underlying glass substrate (see Fig. 7(a) and (b).) The evaluation was conducted at a bending radius of 5 mm and a bending speed of 35 rpm. The transfer characteristics were measured every 10,000 bending cycles for a total of 50,000 bending cycles. Mechanical stress can induce damage to the gate insulator or active layer, thus deteriorating the electrical properties. However, after 50,000 bending cycles, the In_2O_3 TFT fabricated via AP S-ALD maintained a stable electrical performance. However, 50,000 bending cycles in radius environments at 1 mm levels, as in Fig. S5, have deteriorated TFT performance, which is considered to require further research.

4. Conclusions

In this study, we investigated the characteristics of In_2O_3 films grown at 150 °C, 175 °C, 200 °C, and 225 °C via AP S-ALD. To deposit the In_2O_3 films, liquid TMI and O_3 were used as the precursor and reactant, respectively. The effects of N_2 flow separation and substrate velocity on the growth behavior of In_2O_3 were investigated. The self-limiting behavior of the TMI and O_3 was assessed by altering their partial pressures under a 4 slm of N_2 purge gas flow and a substrate velocity of 70 mm/s. Saturation was observed in TMI and O_3 at partial pressures of 70 % or higher and 40 % or higher, respectively. The films exhibited temperature-stable characteristics but a narrow ALD window. As the temperature increased, the growth per cycle (GPC) increases, with the GPC and refractive index reaching values of 1.33 and 2.02, respectively, at 225 °C. To understand the effect of the growth temperature on the characteristics of the In_2O_3 films, we analyzed their electrical properties, contamination, chemical bonding, crystallinity, surface roughness, and density using Hall measurements, XPS, XRD, WAXS, AFM, and XRR. The In_2O_3 thin film indicates a reduction in carrier concentration from $1.53 \pm 1.37 \times 10^{21}$ to $3.09 \pm 0.53 \times 10^{20}$ cm^{-3} as the temperature increased, and a decrease in the resistance from $3.55 \pm 0.07 \times 10^{-3}$ to $3.70 \pm 0.01 \times 10^{-4}$ Ω•cm, which is attributed to a decrease in the impurity concentration (150 °C: 1.5 at.%; 175 °C: 1.0 at.%; 200 °C: N/A; 225 °C: N/A) and an increase in crystallinity (150 °C: 6.56 g/cm^3; 175 °C: 6.85 g/cm^3; 200 °C: 7.00 g/cm^3; 225 °C: 7.09 g/cm^3). We use the In_2O_3 film as a channel layer in a top-gate bottom-contact thin-film transistor (TG-BC

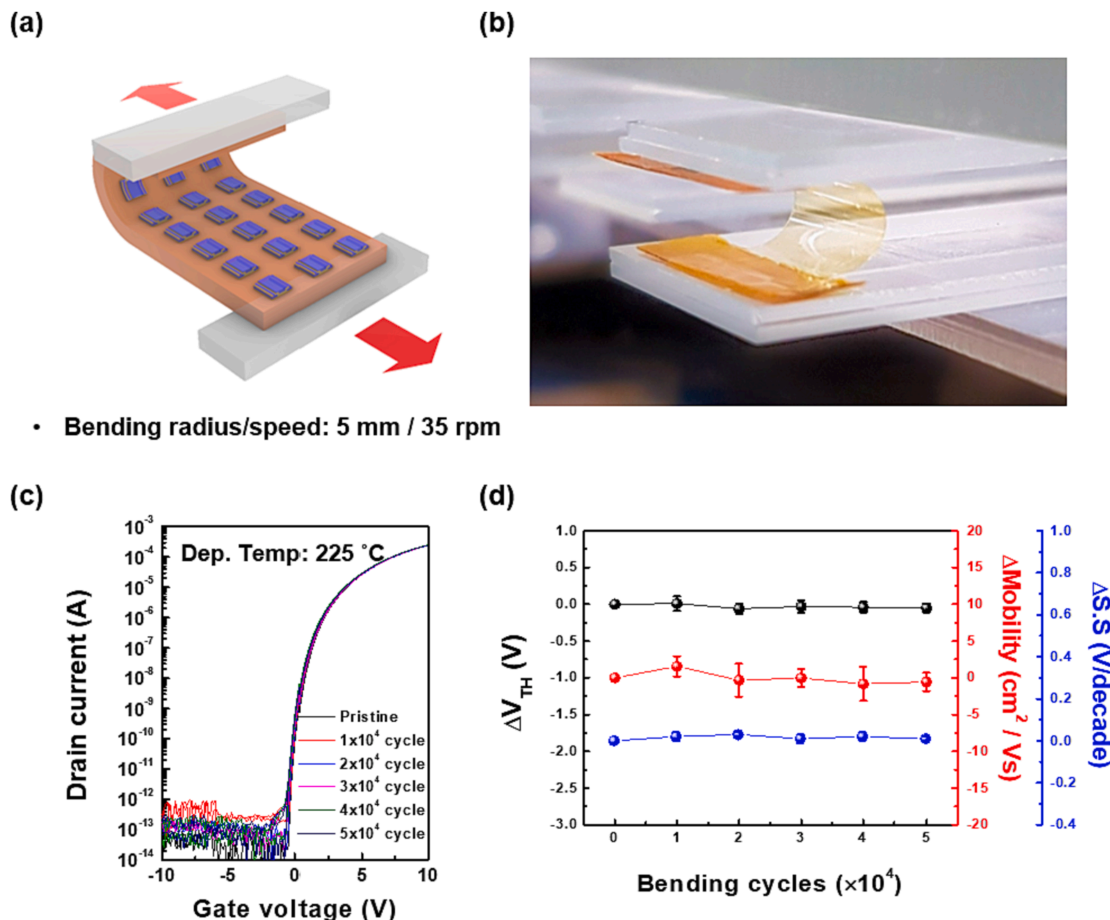

Fig. 7. AP S-ALD-fabricated In_2O_3 TFT: (a) Schematic illustration and (b) photograph during mechanical bending test; and (c) transfer characteristics and (d) electrical parameter variations as a function of bending cycle time. The AP S-ALD-fabricated TFT show negligible change in electrical properties after 50,000 bending cycles.

TFT). The device shows excellent performance characteristics, including a field-effect mobility of 69.8 $cm^2/V{\cdot}s$, a threshold voltage of -0.06 ± 0.22 V, and a subthreshold swing of 0.16 ± 0.01 V/decade. We successfully fabricated high-mobility TFTs and demonstrated their reliability via bias and 50,000 bending tests.

Author contributions

K. S. Yoo and C.-H Lee contributed equally to this study. K. S. Yoo, C.-H Lee, D.-G Kim, S.-H Choi, W.-B. Lee, C.-K. Park and J.-S. Park designed a method for evaluating In_2O_3 films with increasing temperature using AP S-ALD. Lee and Yoo deposited and analyzed thin films. D.-G. Kim and S.-H. Choi et al. fabricated the devices and measured their electrical characteristics. W.-B. Lee prepared a PI substrated and delaminated flexible TFT devices. C. K. Park refabricated flexible In_2O_3 TFT and performed electrical measurement under the mechanical stress conditions. The manuscript was written with contributions from all the authors.

CRediT authorship contribution statement

Kwang Su Yoo: Methodology, Investigation. **Chi-Hoon Lee:** Investigation, Formal analysis. **Dong-Gyu Kim:** Data curation. **Su-Hwan Choi:** Methodology, Investigation. **Won-Bum Lee:** Formal analysis, Data curation. **Chang-Kyun Park:** Investigation, Methodology, Writing – review & editing. **Jin-Seong Park:** Conceptualization, Methodology, Writing – review & editing, Supervision, Project administration.

Declaration of Competing Interest

The authors declare that they have no known competing financial interests or personal relationships that could have appeared to influence the work reported in this paper.

Data availability

Data will be made available on request.

Acknowledgements

This study was supported by the Industry Technology R&D Program (#20010371, #20017382, #20010690), which was funded by the Ministry of Trade, Industry & Energy (MOTIE, Korea) and the National Research Foundation of Korea (NRF) grant funded by the Korea government (MSIT) (No. RS-2023-00260527).

Appendix A. Supplementary material

Supplementary data to this article can be found online at https://doi.org/10.1016/j.apsusc.2023.158950.

References

[1] J. Haeberle, M. Richter, Z. Galazka, C. Janowitz, D. Schmeißer, Resonant photoemission at the O1s threshold to characterize In 2O3 single crystals, Thin Solid Films 555 (2014) 53–56, https://doi.org/10.1016/j.tsf.2013.03.036.
[2] C. Shen, Z. Yin, F. Collins, N. Pinna, Atomic layer deposition of metal oxides and chalcogenides for high performance transistors, Adv. Sci. 9 (2022) 1–37, https://doi.org/10.1002/advs.202104599.
[3] T. Kamiya, K. Nomura, H. Hosono, Present status of amorphous In-Ga-Zn-O thin-film transistors, Sci. Technol. Adv. Mater. 11 (2010), https://doi.org/10.1088/1468-6996/11/4/044305.
[4] P.D.C. King, T.D. Veal, Conductivity in transparent oxide semiconductors, J. Phys. Condens. Matter 23 (2011), 334214, https://doi.org/10.1088/0953-8984/23/33/334214.
[5] P.D.C. King, T.D. Veal, F. Fuchs, C.Y. Wang, D.J. Payne, A. Bourlange, H. Zhang, G. R. Bell, V. Cimalla, O. Ambacher, R.G. Egdell, F. Bechstedt, C.F. McConville, Band gap, electronic structure, and surface electron accumulation of cubic and rhombohedral In2O3, Phys. Rev. B - Condens. Matter Mater. Phys. 79 (2009), 205211, https://doi.org/10.1103/PhysRevB.79.205211.
[6] D. Beena, K.J. Lethy, R. Vinodkumar, A.P. Detty, V.P. Mahadevan Pillai, V. Ganesan, Photoluminescence in laser ablated nanostructured indium oxide thin films, J. Alloy. Compd. 489 (2010) 215–223, https://doi.org/10.1016/j.jallcom.2009.09.055.
[7] R. Mientus, K. Ellmer, Reactive magnetron sputtering of tin-doped indium oxide (ITO): influence of argon pressure and plasma excitation mode, Surf. Coatings Technol. 142 (2001) 748–754, https://doi.org/10.1016/S0257-8972(01)01160-4.
[8] K. Arshak, G. Hickey, E. Forde, J. Harris, Development of a room temperature thin film In2O3, ZnO and SnO2 ozone sensor, (2007) 1536–1541, doi: 10.1109/ISIE.2007.4374831.
[9] C. Cantalini, W. Wlodarski, H.T. Sun, M.Z. Atashbar, M. Passacantando, S. Santucci, NO2 response of In2O3 thin film gas sensors prepared by sol–gel and vacuum thermal evaporation techniques, Sens. Actuators, B 65 (2000) 101–104, https://doi.org/10.1016/S0925-4005(99)00439-6.
[10] L. Francioso, A. Forleo, S. Capone, M. Epifani, A.M. Taurino, P. Siciliano, Nanostructured In2O3-SnO2 sol-gel thin film as material for NO2 detection, Sensors Actuators, B Chem. 114 (2006) 646–655, https://doi.org/10.1016/j.snb.2005.03.124.
[11] G. Wu, Y. Zhou, Y. Ding, T. Yin, Preparation of ITO thin films by injection ultrasound spray pyrolysis and its physical properties, Integr. Ferroelectr. 144 (2013) 161–168, https://doi.org/10.1080/10584587.2013.787842.
[12] X. Xu, D. Wang, J. Liu, P. Sun, Y. Guan, H. Zhang, Y. Sun, F. Liu, X. Liang, Y. Gao, G. Lu, Template-free synthesis of novel In2O3 nanostructures and their application to gas sensors, Sensors Actuators, B Chem. 185 (2013) 32–38, https://doi.org/10.1016/j.snb.2013.04.078.
[13] Z. Yuan, X. Zhu, X. Wang, X. Cai, B. Zhang, D. Qiu, H. Wu, Annealing effects of In2O3 thin films on electrical properties and application in thin film transistors, Thin Solid Films 519 (2011) 3254–3258, https://doi.org/10.1016/j.tsf.2010.12.022.
[14] F. Gherendi, M. Nistor, N.B. Mandache, In2O3 thin film paper transistors, IEEE/OSA J. Disp. Technol. 9 (2013) 760–763, https://doi.org/10.1109/JDT.2013.2278036.
[15] S. Karthikeyan, A.E. Hill, R.D. Pilkington, The deposition of low temperature sputtered In2O3 films using pulsed d.c magnetron sputtering from a powder target, Thin Solid Films 550 (2014) 140–144, https://doi.org/10.1016/j.tsf.2013.10.141.
[16] F. Yang, J. Ma, C. Luan, L. Kong, Structural and optical properties of Ga2(1–x)In2xO3 films prepared on α-Al2O3(0001) by MOCVD, Appl. Surf. Sci. 255 (2009) 4401–4404, https://doi.org/10.1016/j.apsusc.2008.10.129.
[17] R. Yang, J. Zheng, J. Huang, X.Z. Zhang, J.L. Qu, X.G. Li, Low-temperature growth of vertically aligned In2O3 nanoblades with improved lithium storage properties, Electrochem. Commun. 12 (2010) 784–787, https://doi.org/10.1016/j.elecom.2010.03.033.
[18] G. Shen, B. Liang, X. Wang, H. Huang, D. Chen, Z.L. Wang, Ultrathin In2O3 nanowires with diameters below 4 nm: synthesis, reversible wettability switching behavior, and transparent thin-film transistor applications, ACS Nano 5 (2011) 6148–6155, https://doi.org/10.1021/nn2014722.
[19] T.Y. Chou, Y. Chi, S.F. Huang, C.S. Liu, A.J. Carty, L. Scoles, K.A. Udachin, Fluorinated aminoalkoxide and ketoiminate indium complexes as MOCVD precursors for In2O3 thin film deposition, Inorg. Chem. 42 (2003) 6041–6049, https://doi.org/10.1021/ic034588x.
[20] C. Brahim, F. Chauveau, A. Ringuedé, M. Cassir, M. Putkonen, L. Niinistö, ZrO2-In2O3 thin layers with gradual ionic to electronic composition synthesized by atomic layer deposition for SOFC applications, J. Mater. Chem. 19 (2009) 760–766, https://doi.org/10.1039/b813001a.
[21] O. Nilsen, R. Balasundaraprabhu, E.V. Monakhov, N. Muthukumarasamy, H. Fjellvåg, B.G. Svensson, Thin films of In2O3 by atomic layer deposition using In(acac)3, Thin Solid Films 517 (2009) 6320–6322, https://doi.org/10.1016/j.tsf.2009.02.059.
[22] M. Gebhard, M. Hellwig, H. Parala, K. Xu, M. Winter, A. Devi, Indium-tris-guanidinates: A promising class of precursors for water assisted atomic layer deposition of In2O3 thin films, Dalt. Trans. 43 (2014) 937–940, https://doi.org/10.1039/c3dt52746h.
[23] D.-J. Lee, J.-Y. Kwon, J. Il Lee, K.-B. Kim, Self-limiting film growth of transparent conducting In2O3 by atomic layer deposition using trimethylindium and water vapor, J. Phys. Chem. C 115 (2011) 15384–15389, https://doi.org/10.1021/jp2024389.
[24] A. Illiberi, I. Katsouras, S. Gazibegovic, B. Cobb, E. Nekovic, W. van Boekel, C. Frijters, J. Maas, F. Roozeboom, Y. Creyghton, P. Poodt, G. Gelinck, Atmospheric plasma-enhanced spatial-ALD of InZnO for high mobility thin film transistors, J. Vac. Sci. Technol. A Vacuum, Surfaces, Film. 36 (2018) 04F401, https://doi.org/10.1116/1.5008464.
[25] P. Poodt, D.C. Cameron, E. Dickey, S.M. George, V. Kuznetsov, G.N. Parsons, F. Roozeboom, G. Sundaram, A. Vermeer, Spatial atomic layer deposition: A route towards further industrialization of atomic layer deposition, J. Vac. Sci. Technol. A Vacuum, Surfaces, Film. 30 (2012), 010802, https://doi.org/10.1116/1.3670745.
[26] R. Kobayashi, T. Nabatame, K. Kurishima, T. Onaya, A. Ohi, N. Ikeda, T. Nagata, K. Tsukagoshi, A. Ogura, Characteristics of oxide TFT using carbon-doped In2O3 thin film fabricated by low-temperature ALD using ethylcyclopentadienyl indium (In-EtCp) and H2O & O3, ECS Trans. 92 (2019) 3–13, https://doi.org/10.1149/09203.0003ecst.
[27] S.-H. Moon, S.-H. Bae, Y.-H. Kwon, N.-J. Seong, K.-J. Choi, S.-M. Yoon, Combination of InZnO/InGaZnO Bi-layered channels prepared by atomic layer deposition and ozone-based gate-stack formation for guaranteeing high field-effect mobility and long-term stability of thin film transistors, Ceram. Int. 48 (2022) 20905–20913, https://doi.org/10.1016/j.ceramint.2022.04.082.

[28] W.J. Maeng, D.-W. Choi, K.-B. Chung, W. Koh, G.-Y. Kim, S.-Y. Choi, J.-S. Park, Highly conducting, transparent, and flexible indium oxide thin film prepared by atomic layer deposition using a new liquid precursor Et2InN(SiMe3)2, ACS Appl. Mater. Interfaces 6 (2014) 17481–17488, https://doi.org/10.1021/am502085c.

[29] W.J. Maeng, D.-W. Choi, J. Park, J.-S. Park, Indium oxide thin film prepared by low temperature atomic layer deposition using liquid precursors and ozone oxidant, J. Alloy. Compd. 649 (2015) 216–221, https://doi.org/10.1016/j.jallcom.2015.07.150.

[30] T.H. Hong, H.-J. Jeong, H.-M. Lee, S.-H. Choi, J.H. Lim, J.-S. Park, Significance of pairing In/Ga precursor structures on PEALD InGaOxthin-film transistor, ACS Appl. Mater. Interfaces 13 (2021) 28493–28502, https://doi.org/10.1021/acsami.1c06575.

[31] W.J. Maeng, D. Choi, J. Park, J.-S. Park, Atomic layer deposition of highly conductive indium oxide using a liquid precursor and water oxidant, Ceram. Int. 41 (2015) 10782–10787, https://doi.org/10.1016/j.ceramint.2015.05.015.

[32] K.S. Yoo, D.-G. Kim, S. Lee, W.-B. Lee, J.-S. Park, Atmospheric pressure spatial ALD of Al2O3 thin films for flexible PEALD IGZO TFT application, Ceram. Int. 48 (2022) 18803–18810, https://doi.org/10.1016/j.ceramint.2022.03.157.

[33] P. Ryan Fitzpatrick, Z.M. Gibbs, S.M. George, Evaluating operating conditions for continuous atmospheric atomic layer deposition using a multiple slit gas source head, J. Vac. Sci. Technol. A Vacuum, Surfaces, Film. 30 (2012) 01A136, https://doi.org/10.1116/1.3664765.

[34] Z. Deng, W. He, C. Duan, R. Chen, B. Shan, Mechanistic modeling study on process optimization and precursor utilization with atmospheric spatial atomic layer deposition, J. Vac. Sci. Technol. A Vacuum, Surfaces, Film. 34 (2016) 01A108, https://doi.org/10.1116/1.4932564.

[35] V.H. Nguyen, A. Sekkat, C. Jiménez, D. Muñoz, D. Bellet, D. Muñoz-Rojas, Impact of precursor exposure on process efficiency and film properties in spatial atomic layer deposition, Chem. Eng. J. 403 (2021), 126234, https://doi.org/10.1016/j.cej.2020.126234.

[36] S.-H. Choi, T. Hong, S.-H. Ryu, J.-S. Park, Plasma-enhanced atomic-layer-deposited indium oxide thin film using a DMION precursor within a wide process window, Ceram. Int. 48 (2022) 27807–27814, https://doi.org/10.1016/j.ceramint.2022.06.083.

[37] T. Hong, K. Kim, S.-H. Choi, S.-H. Lee, K.-L. Han, J.H. Lim, J.-S. Park, Structural, optical, and electrical properties of inoxthin films deposited by plasma-enhanced atomic layer deposition for flexible device applications, ACS Appl. Electron. Mater. 4 (2022) 3010–3017, https://doi.org/10.1021/acsaelm.2c00434.

[38] A.U. Mane, A.J. Allen, R.K. Kanjolia, J.W. Elam, Indium oxide thin films by atomic layer deposition using trimethylindium and ozone, J. Phys. Chem. C 120 (2016) 9874–9883, https://doi.org/10.1021/acs.jpcc.6b02657.

[39] Y.-S. Shiah, K. Sim, Y. Shi, K. Abe, S. Ueda, M. Sasase, J. Kim, H. Hosono, Mobility–stability trade-off in oxide thin-film transistors, Nat. Electron. 4 (2021) 800–807, https://doi.org/10.1038/s41928-021-00671-0.

[40] C. Wang, L. Yin, L. Zhang, D. Xiang, R. Gao, Metal oxide gas sensors: sensitivity and influencing factors, Sensors 10 (2010) 2088–2106, https://doi.org/10.3390/s100302088.

[41] M.V. Hohmann, P. Goston, A. Wachau, T.J.M. Bayer, J. Brötz, K. Albe, A. Klein, Orientation dependent ionization potential of In2O3: A natural source for inhomogeneous barrier formation at electrode interfaces in organic electronics, J. Phys. Condens. Matter 23 (2011), https://doi.org/10.1088/0953-8984/23/33/334203.

[42] D.B. Buchholz, Q. Ma, D. Alducin, A. Ponce, M. Jose-Yacaman, R. Khanal, J. E. Medvedeva, R.P.H. Chang, The structure and properties of amorphous indium oxide, Chem. Mater. 26 (2014) 5401–5411, https://doi.org/10.1021/cm502689x.

[43] Y.H. Hsiao, H.T. Lue, W.C. Chen, K.P. Chang, Y.H. Shih, B.Y. Tsui, K.Y. Hsieh, C. Y. Lu, Modeling the impact of random grain boundary traps on the electrical behavior of vertical gate 3-D NAND flash memory devices, IEEE Trans. Electron Devices 61 (2014) 2064–2070, https://doi.org/10.1109/TED.2014.2318716.

[44] A. Bolognesi, M. Berliocchi, M. Manenti, A. Di Carlo, P. Lugli, K. Lmimouni, C. Dufour, Effects of grain boundaries, field-dependent mobility, and interface trap states on the electrical characteristics of pentacene TFT, IEEE Trans. Electron Devices 51 (2004) 1997–2003, https://doi.org/10.1109/TED.2004.838333.

[45] Y. Jeong, C. Bae, D. Kim, K. Song, K. Woo, H. Shin, G. Cao, J. Moon, Bias-stress-stable solution-processed oxide thin film transistors, ACS Appl. Mater. Interfaces 2 (2010) 611–615, https://doi.org/10.1021/am900787k.

[46] H.-K. Noh, K.J. Chang, B. Ryu, W.J. Lee, Electronic structure of oxygen-vacancy defects in amorphous In-Ga-Zn-O semiconductors, Phys. Rev. B - Condens. Matter Mater. Phys. 84 (2011), 115205, https://doi.org/10.1103/PhysRevB.84.115205.